Chinese Chemical Letters 35 (2024) 109156

Contents lists available at ScienceDirect

Chinese Chemical Letters

journal homepage: www.elsevier.com/locate/cclet

A near-infrared fluorescent probe for visualizing transformation pathway of Cys/Hcy and H_2S and its applications in living system

Yudi Cheng[a,b,1], Xiao Wang[a,1], Jiao Chen[a,b], Zihan Zhang[a], Jiadong Ou[a], Mengyao She[a,b], Fulin Chen[b,*], Jianli Li[a,*]

[a] Key Laboratory of Synthetic and Natural Functional Molecule of the Ministry of Education, Xi'an Key Laboratory of Functional Supramolecular Structure and Materials, College of Chemistry & Materials Science, Northwest University, Xi'an 710127, China
[b] Key Laboratory of Resource Biology and Biotechnology in Western China, Ministry of Education, Biomedicine Key Laboratory of Shaanxi Province, Lab of Tissue Engineering, the College of Life Sciences, Faculty of Life Science & Medicine, Northwest University, Xi'an 710069, China

ARTICLE INFO

Article history:
Received 2 August 2023
Revised 23 September 2023
Accepted 25 September 2023
Available online 27 September 2023

Keywords:
Fluorescent probe
Near-infrared
Hydrogen sulfide
Cysteine/homocysteine
Large Stokes shift
Dicyanoisophorone
Drug-induced liver injury

ABSTRACT

Sulfydryl-contained (-SH) substances including hydrogen sulfide (H_2S), cysteine (Cys), homocysteine (Hcy) and glutathione (GSH) play crucial roles in living systems, and their variations are closely associated with various diseases. Herein, we developed a near-infrared intramolecular charge transfer (ICT) based fluorescent probe **Y-NBD**, achieving detection of Cys/Hcy and H_2S with different fluorescent signals (green-red for Cys/Hcy, red for H_2S), large Stokes shifts (~100/105 nm or 191 nm) and high signal-background-ratio, but not responding to GSH. **Y-NBD** was successfully applied to image exogenous/endogenous Cys/Hcy and H_2S in various living cancer cells (HeLa, A549, and HepG2) and in zebrafish. It not only visualized the transformation pathway of several thiols in HepG2 cells but also verified that the intestine is the main site for the activation and metabolism of **Y-NBD** in zebrafish, as well as realized to evaluate the degree of drug-induced liver injury. This work provides a promising tool for imaging Cys/Hcy and H_2S in living systems and shows great potency in evaluating drug-induced liver injury and its treatment.

Sulfydryl-contained (-SH) substances, namely biothiols, including hydrogen sulfide (H_2S), cysteine (Cys), homocysteine (Hcy) and glutathione (GSH) are important reductants in living systems, which are crucial in maintaining redox homeostasis and participating in signal transduction [1–5]. H_2S is the third vital signaling molecule after carbon monoxide (CO) and nitric oxide (NO) in living system, and it is produced from Cys and Hcy *via* enzymatic metabolism of cystathionine γ-lyase (CSE), cystathionine β-synthase (CBS), and 3-mercaptopyruvate sulfurtransferase (3-MST) [6–9]. In signaling processes, there is a rapid fluctuation in the concentration of endogenous H_2S from nanomolar to sub millimolar levels [10]. Generally, the abnormal variation of H_2S is associated with acute liver/lung injury [11,12], nonalcoholic fatty liver [13,14], Alzheimer's disease [15], Parkinson's disease [16], inflammation [17], cancer [18,19], *etc*. Cys/Hcy/GSH are considered the most abundant biothiols, which are found in the concentration ranges of 240–360 μmol/L (Cys), 12–15 μmol/L (Hcy), and 1–10 mmol/L (GSH) in living beings [20]. The abnormal fluctuations of Cys/Hcy/GSH are associated with liver damage [21,22], muscle loss [23], diabetes [24], atherosclerotic cardiovascular disease [25], cancer [26,27], epilepsy [28], *etc*. As depicted in Fig. 1b, H_2S and Cys/Hcy/GSH formed a transformation network in organism, which highlights the importance of distinguishing H_2S and Cys/Hcy/GSH to understand their transformation network, metabolic process and the related pathological characteristics.

The fluorescent probe, especially the activatable near-infrared (NIR) fluorescent probe, has attracted tremendous concerns due to the merits of high sensitivity, low background signal, real-time and *in-situ* imaging [29–36]. In the past decades, a large number of Cys/Hcy/GSH and H_2S specific fluorescent probes have been reported based on the mechanism of nucleophilic aromatic substitution reaction (S_NAr) [37–39]. However, owing to their similar reactivity and rapid transformation in living systems, dynamic differentiating biothiols by one probe is still challenging. In fact, -SH-contained substances have different pK_a values (6.9 (H_2S), 8.3 (Cys), 8.9 (Hcy), and 9.2 (GSH)) [40], which suggests that H_2S has a stronger nucleophilicity than other biothiols. Based on this, some fluorescent probes were reported for selective detection of single thiol [39], or simultaneous detection of Cys/Hcy/GSH/H_2S with

* Corresponding authors.
E-mail addresses: chenfl@nwu.edu.cn (F. Chen), lijianli@nwu.edu.cn (J. Li).
[1] These authors contributed equally to this work.

https://doi.org/10.1016/j.cclet.2023.109156
1001-8417/

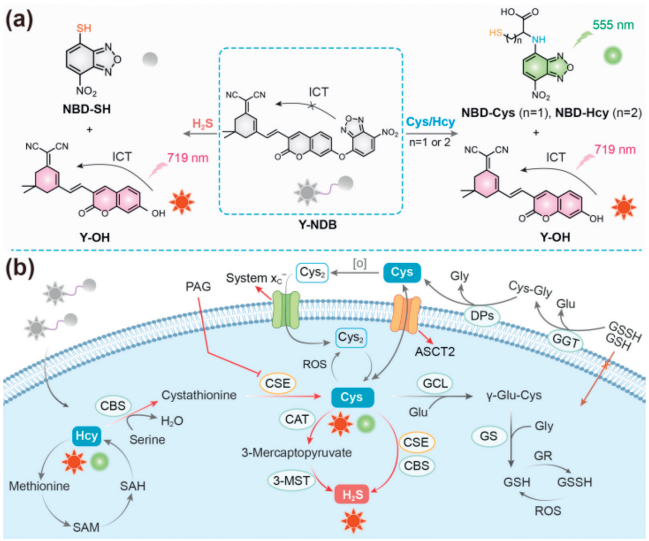

Fig. 1. (a) Mechanism of **Y-NBD** responding to Cys/Hcy and H_2S in this work. (b) Schematic diagram of the mutual conversion of Hcy/Cys and the generation of H_2S. The abbreviations in Fig. 1b are presented in Supporting information.

multiple fluorescent signals [41,42]. Nevertheless, the NIR fluorescence probe that simultaneously responds to Cys/Hcy and H_2S with high signal-background-ratio (SBR) without recognizing GSH has rarely been reported.

In this work, we constructed an intramolecular charge transfer (ICT)-based NIR fluorescent probe **Y-NBD** by using dicyanoisophorone-coumarin as fluorophore and 7-nitro-1,2,3-benzoxadiazole (NBD) as recognition unit. **Y-NBD** exhibits high selectivity towards Cys/Hcy and H_2S (Fig. 1a), showing excellent capability of imaging the exogenous/endogenous thiols in various living cells and zebrafish. Furthermore, **Y-NBD** shows a certain potency to investigate variations of Cys/Hcy and H_2S in drug-induced liver injury and its remediation.

To design a NIR fluorescent probe for the differentiation of several biothiols with high SBR, the ICT mechanism was chosen to regulate the fluorescence. First, the dicyanoisophorone [43] was selected to bridge the aldehyde coumarin derivative to enlarge the conjugation system forming the fluorophore **Y-OH**, which would be an ICT-controllable NIR fluorophore with a large Stokes shift. NBD chromophore, as recognition unit and fluorescence masking unit, was linked to fluorophore **Y-OH** a by an ether bond to obtain probe **Y-NBD** (Fig. S1 in Supporting information), and its characteristic data were presented in Supporting information.

With the targeted probe **Y-NBD** in hand, its recognition selectivity was first examined by absorption and fluorescence spectra. The absorption spectra of **Y-NBD** displayed significant changes upon addition of Cys/Hcy and H_2S. As shown in Fig. 2a, the **Y-NBD** shows a ~55 nm redshift for Cys/Hcy (100 μmol/L) and a ~140 nm redshift for H_2S (100 μmol/L). Moreover, free **Y-NBD** shows almost no background fluorescence, whereas Cys/Hcy induces remarkable fluorescence signals at 555 nm (Fig. 2b) and H_2S at 719 nm (Fig. 2c) with 30-fold/242-fold and 27-fold enhancement, respectively. Notably, the absorption and fluorescence spectra of **Y-NBD** exhibit negligible changes upon addition of GSH, even the concentration of GSH up to 5 mmol/L (Fig. S2 in Supporting information), indicating that **Y-NBD** can differentiate Cys/Hcy and H_2S with high SBR and indeed cannot respond to GSH.

Subsequently, titration experiments were carried out to check the quantitative capability of **Y-NBD** for Cys/Hcy and H_2S. Absorption of **Y-NBD** exhibited redshift and ratio changes upon addition of various concentrations of Cys/Hcy and H_2S (Figs. S3a–c in Supporting information). Meanwhile, the fluorescence intensity of **Y-NBD** solution at both 555 nm and 719 nm were gradually increased upon addition of Cys/Hcy (0–500 μmol/L) (Figs. 2d and e, Figs. S4a and b in Supporting information) with a linear fit at 0–50 μmol/L for Cys ($R^2 = 0.9909$) and 0–20 μmol/L for Hcy ($R^2 = 0.9948$) (Figs. S5a and b in Supporting information). Simultaneously, as the concentration of H_2S gradually increased (0–500 μmol/L), the fluorescent intensity of **Y-NBD** solution was significantly increased merely at 719 nm with a linear relationship at 0–100 μmol/L ($R^2 = 0.9903$) (Fig. 2f and Fig. S5c in Supporting information). The limits of detection (LOD = 3σ/K) were determined to be 79 nmol/L (Cys), 24 nmol/L (Hcy) and 203 nmol/L (H_2S), suggesting **Y-NBD** is suitable for quantitative detection of low-concentration thiols.

To evaluate the application capability of **Y-NBD** in complex living systems, the anti-interference of **Y-NBD** towards Cys/Hcy and H_2S in presence of other analytes were investigated, indicating that almost no significant fluorescence changes were observed when Cys/Hcy and H_2S coexisted with various species except for HClO, which showed a slight decrease in fluorescence intensity at 555 nm (Figs. S5d–f in Supporting information). It would be ascribed to the oxidizability of HClO causing part inactivation of Cys/Hcy. Considering a relatively low concentration of HClO in the biological system, its interference could be neglected. The effect of pH showed that free **Y-NBD** possesses good pH stability at a wide pH range, while the fluorescence intensity of **Y-NBD** in presence of H_2S showed dramatically increase under alkaline conditions due to the generated compound **Y-OH** existed in "basic form" ($pK_a = 7.62$) (Figs. S6 and S7 in Supporting information). Moreover, time-dependent fluorescence spectra showed that Cys-induced fluorescence increased within 20 min and reached a plateau at 40 min (Fig. 2g), while Hcy was slower than Cys, which increased within 30 min (Fig. 2h). By comparison, H_2S-induced fluorescence intensity increased quickly within 10 min and reached a plateau at 20 min (Fig. 2i), which is attributed to its higher nucleophilicity than Cys/Hcy. More importantly, the Stokes shift of **Y-NBD** for Cys/Hcy and H_2S are 100/105 nm and 191 nm, respectively (Figs. 2j–l). Such a large Stokes shift would effectively avoid false positive signals resulting from excitation light in the application of confocal imaging.

The recognition mechanism was explored and proposed according to the reported work [44–47]. As depicted in Fig. S8a (Supporting information), the -SH group of H_2S/Cys/Hcy reacted with **Y-NBD** *via* S_NAr reaction along with the release of fluorophore **Y-OH**. The intermediate of five/six member-rings formed as a result of recombination between the -NH_2 group and the -SH group of Cys/Hcy. All the reaction products were consistent with the corresponding HRMS data (Fig. S9 in Supporting information), indicating the feasibility of the deduced recognition mechanism. To further explore whether the fluorescent signal was regulated by the ICT process, theoretical calculation was carried out. As illustrated in Fig. S8b (Supporting information), the electrostatic potential (ESP) of **Y-OH** exhibited negative-to-positive (negative in red and positive in blue), which would be well matched with ICT process with dramatical fluorescence, while the ESP of **Y-NBD** showed negative-to-negative, resulting in the break of ICT process with none-fluorescence. In addition, the highest occupied molecular orbital (HOMO) and lowest unoccupied molecular orbital (LUMO) distributions were calculated. Compared with the compound **Y-OH**, the HOMO distribution of **Y-NBD** only was in the plane of the fluorophore, while the LUMO distribution of **Y-NBD** was in both recognition unit and fluorophore (Fig. S8c in Supporting information), suggesting that **Y-NBD** would afford a moderate reactivity for nucleophile species. This is also different from the GSH-specific fluorescent probe that LUMO distribution locates only in the recognition unit [21,48], which properly supported that **Y-NBD** only responds to Cys/Hcy and H_2S, but cannot react with GSH.

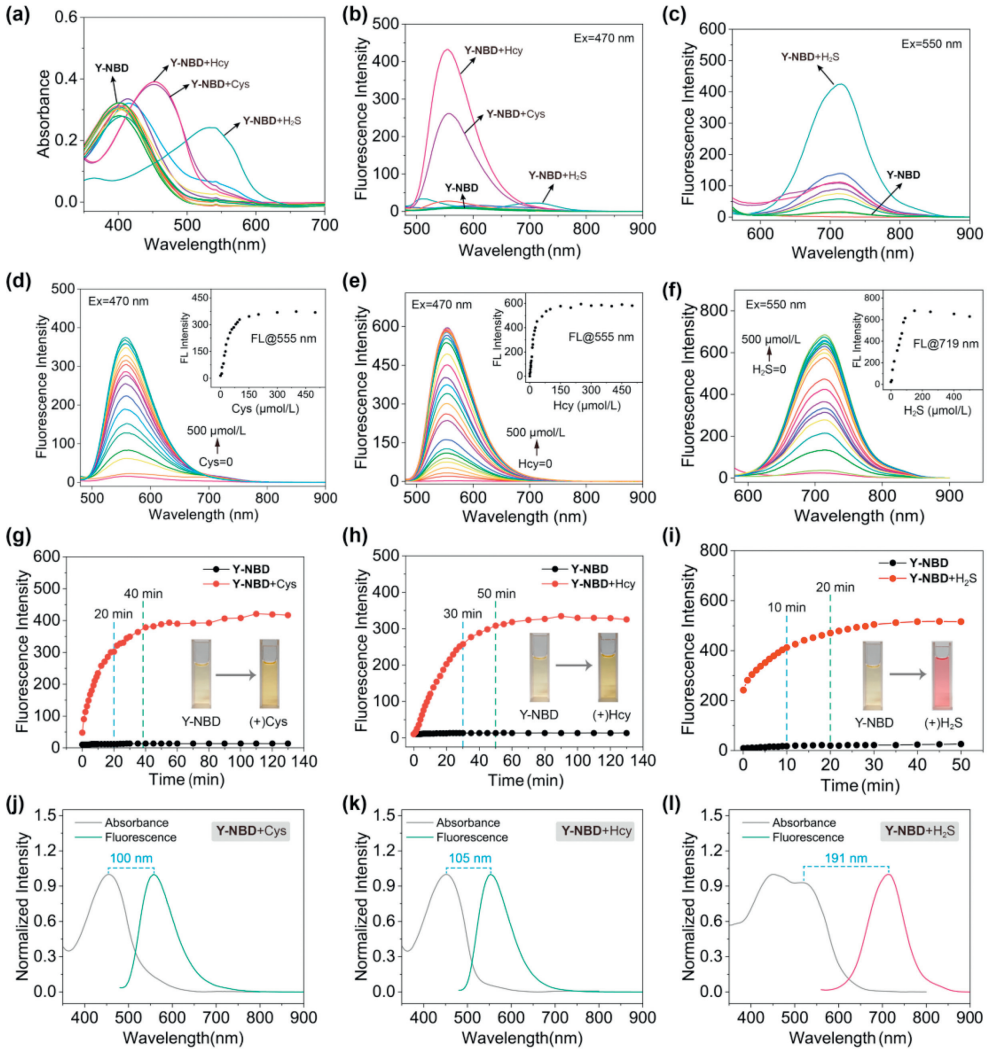

Fig. 2. Ultraviolet absorbance (a) and fluorescence spectra (b, λ_{ex} = 470 nm; c, λ_{ex} = 550 nm) of **Y-NBD** (10 μmol/L) upon addition of Cys/Hcy/H_2S (100 μmol/L) in CH_3CN/PBS (4:6, v/v). (d–f) Fluorescence spectra of **Y-NBD** (10 μmol/L) in presence of various concentrations of Cys/Hcy/H_2S, the insert is the corresponding fluorescent intensity and the concentration of the analyte. (g–i) Time-dependent fluorescence intensity of **Y-NBD** (10 μmol/L) in absence and presence of Cys (100 μmol/L) (g), Hcy (100 μmol/L) (h) at 555 nm and H_2S (100 μmol/L) (i) at 719 nm. (j–l) Stokes shift of **Y-NBD** in presence of Cys (j), Hcy (k), and H_2S (l).

To check the capability of **Y-NBD** to image Cys/Hcy and H_2S in living systems, the cytotoxicity of the **Y-NBD** was first evaluated by MTT assay. As shown in Fig. S10 (Supporting information), the cell viability of living cells (HeLa, A549, and HepG2) were more than 80% after incubation of **Y-NBD** (10 μmol/L) for 24 h, suggesting low toxicity of **Y-NBD**. Subsequently, **Y-NBD** was utilized to image intracellular Cys/Hcy and H_2S. As shown in Fig. S11a (Supporting information), both the green channel and red channel showed significant fluorescence signals in living HeLa, A549, and HepG2 cells. Moreover, it seems that the fluorescent signal in HepG2 cells was higher than that in A549 cells and HeLa cells (Fig. S11b in Supporting information), revealing that HepG2 cells may contain more Cys/Hcy and H_2S than A549 and HeLa cells. Thus, the HepG2 cell was chosen to perform the subsequent experiments.

The distribution and transformation of Cys/Hcy and H_2S in living cells were further investigated. Compared with the cells only incubated with **Y-NBD** (Fig. 3a1), the cells pretreated with *N*-ethylmaleimide (NEM, a thiol scavenger) and then incubated with **Y-NBD** exhibited barely fluorescence signals in both green channel and red channel (Fig. 3a2). Meanwhile, when cells were pretreated with NEM followed by upon addition of Cys/Hcy or H_2S, the fluorescence recovered obviously (Figs. 3a3–a5 and b), indicating that **Y-NBD** could be utilized to monitor exogenous Cys/Hcy and H_2S. In addition, when *N*-acetylcysteine (NAC, a precursor of cysteine) was added to cells before incubation of **Y-NBD**, the fluorescence signals were dramatically increased in both green channel and red channel (Fig. 3a6). Afterward, we explored **Y-NBD** to image endogenous H_2S. Given that CSE is one of the important enzymes to catalyze Cys convert to H_2S [9,49], and DL-propargylglycine (PAG) is a famous inhibitor of CSE [50,51]. We thus used PAG to inhibit CSE to transform Cys into H_2S as a control, which observed a significant decrease of fluorescence in red channel (Fig. 3a7). Moreover, by using GSH to elevate the endogenous Cys and induce H_2S production [52], the fluorescence in the two channels were increased compared with the control group (Figs. 3a8 and b), suggesting it is reasonable to convert Cys or GSH into intracellular H_2S. 3D imaging showed that the fluorescence signals were located intracellular with high SBR (Fig. 3c). The results manifested **Y-NBD** could image endogenous Cys/Hcy and H_2S and illustrate the transformation relationship between several intracellular thiols with excellent imaging performance.

Considering zebrafish and their embryos hold significant potential for advancing research on human diseases because zebrafish possess a high level of genetic homology (approximately 87%) with

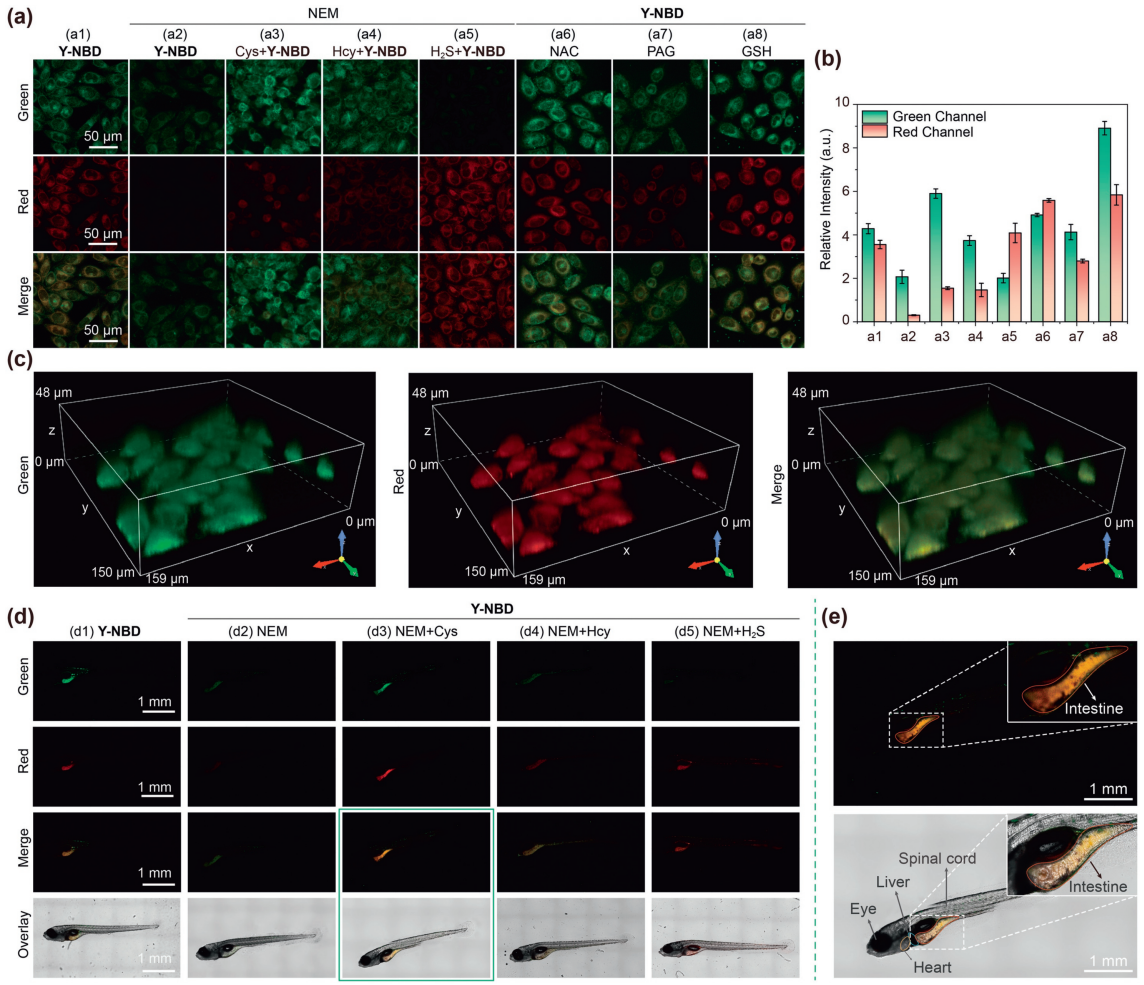

Fig. 3. (a) Confocal images of the detection Cys/Hcy/H_2S in HepG2 cells (Scale bar: 50 μm). (a1) Cells incubated with **Y-NBD**; (a2–a5) cells pretreated with NEM (100 μmol/L, 30 min) followed by incubation with Cys (a3), Hcy (a4), and H_2S (a5) (50 μmol/L, 30 min) and then upon addition of **Y-NBD**; (a6–a8) cells pretreated with NAC (100 μmol/L, 6 h) (a6), PAG (200 μmol/L, 6 h) (a7), GSH (200 μmol/L, 6 h) (a8), and then incubated with **Y-NBD**. (b) Relative fluorescence intensity of Fig. 3a conducted by the software of Image J. (c) Z-axis scanning and three-dimensional reconstruction in green and red channels in living HepG2 cells. (d) Confocal imaging of zebrafish (Scale bar: 1 mm). (d1) Zebrafish incubated with **Y-NBD** (10 μmol/L) for 30 min; (d2) zebrafish treated with NEM (1 mmol/L, 30 min) and then upon addition of **Y-NBD**; (d3–d5) zebrafish pretreated with NEM (1 mmol/L, 30 min) followed by incubation with Cys/Hcy/H_2S (50 μmol/L, 30 min) and then upon addition of **Y-NBD**. (e) Enlargement of merge and overlay in Fig. 3d3.

humans [53,54], the imaging capability of the **Y-NBD** in zebrafish was examined. All the animal experiments have been approved by the Animal Ethics Committee of Northwest University (NWU-AWC-20230403M). As shown in Fig. 3d1, **Y-NBD** exhibited obvious signals in both green and red channels in zebrafish. However, with the pretreatment of NEM, there was almost no fluorescent signal was observed (Fig. 3d2). Meanwhile, when exogenous Cys/Hcy or H_2S were added, the fluorescent signals were observed obviously (Fig. 3d3–d5) and mainly existed in the intestine (Fig. 3e). It manifests that **Y-NBD** exerts well imaging ability for detecting Cys/Hcy and H_2S in zebrafish, and **Y-NBD** would be metabolized through the intestine of zebrafish. Furthermore, given that the concentration of thiols decreases dramatically during drug-induced liver injury (DILI) [11,55–57], we further examined the capability of **Y-NBD** to evaluate DILI. As illustrated in Figs. 4a and b, when cells were pretreated with overdose acetaminophen (APAP, a highly utilized medication for relief of pain and fever but overdose leads to liver injury [58]) followed by the incubation of **Y-NBD**, the fluorescence signals decreased in two channels. However, after treatment of NAC or GSH, the fluorescence showed a significant enhancement in both green and red channels, suggesting that both NAC and GSH have certain efficacy in alleviating liver injury. Besides, the fluorescence intensity of the cells treated with NAC was higher than that treated with GSH, indicating that NAC would be a more efficient drug to treat APAP-induced liver injury.

To check the DILI imaging capability of **Y-NBD** in liver tissue, the biosafety of **Y-NBD** was evaluated first by hematoxylin-eosin (HE) staining. As depicted in Fig. S12 (Supporting information), after administration of **Y-NBD**, no obvious histological morphology changes of main organs (heart, liver, spleen, lung, kidney) were observed compared with the control group, suggesting that the **Y-NBD** has good biosafety *in vivo*. Then the APAP-induced liver injury mice model was constructed to evaluate DILI by using **Y-NBD**. As shown in Fig. 4c2, the liver from the mouse pretreated with overdose-APAP shows a remarkable decrease in fluorescence signal compared with the control group (Fig. 4c1), while a recovered fluorescence signal was observed after being treated with NAC (Fig. 4c3), indicating that **Y-NBD** has a tremendous potency to visualize liver injury and its remediation. Besides, HE and staining and Masson's trichrome (Masson) staining were performed. As shown in Fig. 4c5, the overdose-APAP treated group shows a local aggregation of inflammatory cell infiltration compared with the control group (Fig. 4c4), while after treatment with NAC, this phenomenon reduced obviously (Fig. 4c6). Mas-

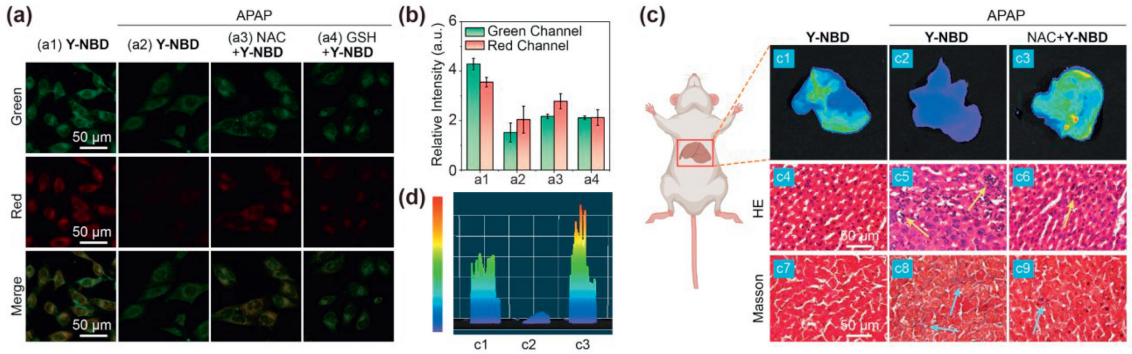

Fig. 4. (a) Fluorescence imaging of APAP-treated cells and remediation (Scale bar: 50 μm). (a1) Cells are incubated with **Y-NBD**; (a2–a4) Cells pretreated with APAP (5 mmol/L) and then upon addition of NAC (1 mmol/L) (a3) or GSH (1 mmol/L) (a4) before incubation of **Y-NBD**. (b) Relative fluorescence intensity of Fig. 4a conducted by the software of Image J. (c) APAP-induced injury liver imaging and HE/Masson staining. (c1) Control group, the liver from normal mouse with intraperitoneal injection of **Y-NBD**. (c2) DILI group, the liver from the mouse pretreated with overdose APAP (350 mg/kg) before intraperitoneal injection of **Y-NBD**. (c3) Remediation group, the liver from the mouse with intraperitoneal injection of NAC (200 mg kg^{-1} d^{-1}) for 5 days, and then intraperitoneal injection of **Y-NBD** (1 mmol/L, 500 μL) 1 h after gavage APAP (350 mg/kg), (yellow arrow: inflammatory cell infiltration; blue arrow: fibrosis in tissues; scale bar: 50 μm). (d) Fluorescence semi-quantitative analysis of Fig. 4c.

son staining shows that the overdose-APAP treated group shows mild fibrosis in the hepatocellular stroma (Fig. 4c8) compared with the control group (Fig. 4c7) and the degree of fibrosis decreased after treatment of NAC (Fig. 4c9). These staining results of HE and Masson further validate the feasibility and accuracy of **Y-NBD** for assessing the degree of DILI and its treatment efficiency of drugs.

In summary, we developed an ICT-based NIR fluorescent probe **Y-NBD** by using dicyanoisophorone-coumarin as fluorophore and nitrobenzoxazole as the recognition unit. **Y-NBD** enables differentiation of Cys/Hcy and H_2S (not responding to GSH) with high SBR and large Stokes shift. It can be applied to visualize exogenous and endogenous Cys/Hcy and H_2S in living cells and zebrafish. The results suggest that HepG2 cells contain more Cys/Hcy and H_2S than other cell lines, and **Y-NBD** is mainly activated and metabolized in the intestine of zebrafish. Moreover, **Y-NBD** was applied to monitor the conversion of Cys/Hcy or GSH into H_2S in living HepG2 cells, as well as assess APAP-induced liver injury and its remediation. This work not only provides a valuable fluorescent probe **Y-NBD** to visualize the transformation pathway of Cys/Hcy and H_2S in living systems but also affords a promising tool for evaluating hepatotoxicity and its treatment efficiency in drug discovery.

Declaration of competing interest

The authors declare that they have no known competing financial interests or personal relationships that could have appeared to influence the work reported in this paper.

Acknowledgments

This work was supported by the National Natural Science Foundation of China (Nos. 22077099 and 22171223), the Innovation Capability Support Program of Shaanxi (Nos. 2023-CX-TD-75 and 2022KJXX-32), the Technology Innovation Leading Program of Shaanxi (Program No. 2023KXJ-209), the Natural Science Basic Research Program of Shaanxi (Nos. 2022JQ-151 and 2023-JC-YB-141), and Young Talent Fund of Association for Science and Technology in Shaanxi, China (No. SWYY202206), the Shaanxi Fundamental Science Research Project for Chemistry & Biology (Nos. 22JHZ010 and 22JHQ080), the Yan'an City Science and Technology Project (No. 2022SLZDCY-002).

Supplementary materials

Supplementary material associated with this article can be found, in the online version, at doi:10.1016/j.cclet.2023.109156.

References

[1] Y. Yue, F. Huo, F. Cheng, et al., Chem. Soc. Rev. 48 (2019) 4155–4177.
[2] B.J. Bezner, L.S. Ryan, A.R. Lippert, Anal. Chem. 92 (2020) 309–326.
[3] Y. Yue, F. Huo, C. Yin, Chem. Sci. 12 (2020) 1220–1226.
[4] K. Ma, H. Yang, T. Shen, et al., Chem. Sci. 13 (2022) 3706–3712.
[5] W. Zhang, F. Huo, F. Cheng, et al., J. Am. Chem. Soc. 142 (2020) 6324–6331.
[6] S. Singh, D. Padovani, R.A. Leslie, et al., J. Biol. Chem. 284 (2009) 22457–22466.
[7] B. Fowler, Semin. Vasc. Med. 5 (2005) 77–86.
[8] G. Caliendo, G. Cirino, V. Santagada, et al., J. Med. Chem. 53 (2010) 6275–6286.
[9] V.D.B. Bonifacio, S.A. Pereira, J. Serpa, et al., Br. J. Cancer 124 (2021) 862–879.
[10] B. Ke, W. Wu, W. Liu, et al., Anal. Chem. 88 (2016) 592–595.
[11] K. Wang, R. Guo, X.Y. Chen, et al., Chem. Eng. J. 468 (2023) 143611.
[12] W. Su, L. Huang, L. Zhu, et al., Sens. Actuat. B: Chem. 369 (2022) 132297.
[13] Y. Shen, Q. Zhou, W. Li, et al., Chem. Asian. J. 17 (2022) e202200320.
[14] W. Li, Y. Shen, X. Gong, et al., Anal. Chem. 93 (2021) 16673–16682.
[15] P. Sun, H.C. Chen, S. Lu, et al., Anal. Chem. 94 (2022) 11573–11581.
[16] S.K. Bae, C.H. Heo, D.J. Choi, et al., J. Am. Chem. Soc. 135 (2013) 9915–9923.
[17] S. Gong, Z. Zheng, X. Guan, et al., Anal. Chem. 93 (2021) 5700–5708.
[18] X. Dong, L. Sun, Z. Zhang, et al., Sci. China Chem. 66 (2023) 1869–1876.
[19] Y. Zhang, J. Fang, S. Ye, et al., Nat. Commun. 13 (2022) 1685.
[20] R. Kaushik, N. Nehra, V. Novakova, et al., ACS Omega 8 (2023) 98–126.
[21] J. Chen, Z. Wang, M. She, et al., ACS Appl. Mater. Interfaces 11 (2019) 32605–32612.
[22] J. Chen, D. Huang, M. She, et al., ACS Sens. 6 (2021) 628–640.
[23] P. Zhou, M. She, P. Liu, et al., Sens. Actuat. B: Chem. 318 (2020) 128258.
[24] G. Yin, Y. Gan, H. Jiang, et al., Anal. Chem. 95 (2023) 8932–8938.
[25] F. Wei, Y. Ding, J. Ou, et al., Anal. Chem. 95 (2023) 9173–9181.
[26] Y. Huang, Y. Zhang, F. Huo, et al., J. Am. Chem. Soc. 142 (2020) 18706–18714.
[27] H. Yan, F. Huo, Y. Yue, et al., J. Am. Chem. Soc. 143 (2020) 318–325.
[28] S. Li, P. Wang, M. Ye, et al., Anal. Chem. 95 (2023) 5133–5141.
[29] W. Dou, H. Han, A. Sedgwick, et al., Sci. Bull. 67 (2022) 853–878.
[30] L. Chen, Y. Lyu, X. Zhang, et al., Sci. China Chem. 66 (2023) 1336–1383.
[31] H. Fang, Y. Chen, Z. Jiang, et al., Acc. Chem. Res. 56 (2023) 258–269.
[32] J. Yin, J. Zhan, Q. Hu, et al., Chem. Soc. Rev. 52 (2023) 2011–2030.
[33] Z. Wang, J. Li, J. Chen, et al., Chin. Chem. Lett. 34 (2023) 108507.
[34] X. Ma, Y. Huang, W. Chen, et al., Angew. Chem. Int. Ed. 62 (2023) e202216109.
[35] H. Zhang, C. He, L. Shen, et al., Chin. Chem. Lett. 34 (2023) 108160.
[36] D. Li, T. Shen, X. Xue, et al., Sci. China Chem. 66 (2023) 2329–2338.
[37] L. Kong, W. Lu, X. Cao, et al., J. Mater. Chem. B 10 (2022) 7924–7954.
[38] Z. Xu, T. Qin, X. Zhou, et al., Trend. Anal. Chem. 121 (2019) 115672.
[39] X. Jiao, Y. Li, J. Niu, et al., Anal. Chem. 90 (2018) 533–555.
[40] L. Yang, Y. Su, Y. Geng, et al., ACS Sens. 3 (2018) 1863–1869.
[41] C. Yin, K. Xiong, F. Huo, et al., Angew. Chem. Int. Ed. 56 (2017) 13188–13198.
[42] S. Li, F. Huo, Y. Yue, et al., Chin. Chem. Lett. 32 (2021) 3870–3875.
[43] L. Dai, Q. Zhang, Q. Ma, et al., Coord. Chem. Rev. 489 (2023) 215193.
[44] Y. Zheng, Z. Chai, W. Tang, et al., Sens. Actuat. B: Chem. 330 (2021) 129343.
[45] S. Ding, W. Feng, G. Feng, Sens. Actuat. B: Chem. 238 (2017) 619–625.
[46] Y. Kang, L. Niu, Q. Yang, Chin. Chem. Lett. 30 (2019) 1791–1798.
[47] Y. Kim, J. Kim, J.M. An, et al., ACS Sens. 8 (2023) 1723–1732.
[48] J. Chen, Y. Li, X. Feng, et al., Spectrochim. Acta A: Mol. Biomol. Spectrosc. 246 (2021) 119041.
[49] S.E. Wilkie, G. Borland, R.N. Carter, et al., Biochem. J. 478 (2021) 3485–3504.

[50] R. Montanaro, V. Vellecco, R. Torregrossa, et al., Redox Biol. 62 (2023) 102657.
[51] H.M.S. Al Ubeed, R.B.H. Wills, M.C. Bowyer, et al., Postharvest Biol. Technol. 147 (2019) 54–58.
[52] P. Zhang, X. Nie, M. Gao, et al., Mater. Chem. Front. 1 (2017) 838–845.
[53] X. Wang, J. Zhang, K. He, et al., Front. Pharmacol. 12 (2021) 713963.
[54] S.M. Alavi Naini, N. Soussi-Yanicostas, Front. Cell Dev. Biol. 6 (2018) 163.
[55] Y. Yang, K. Zhou, M. Ma, et al., Chem. Eng. J. 452 (2023) 139020.
[56] C. Srinivasan, W.M. Williams, H.T. Nagasawa, et al., Biochem. Pharmacol. 61 (2001) 925–931.
[57] R. Chen, W. Li, R. Li, et al., Chin. Chem. Lett. 34 (2023) 107845.
[58] W.M. Lee, J. Hepatol. 67 (2017) 1324–1331.